

# Waveshape tolerant photonic quantum gates

I. Babushkin,<sup>1,2,3</sup> A. Demircan,<sup>1,3</sup> M. Kues,<sup>3,4</sup> and U. Morgner<sup>1,3</sup>

<sup>1</sup>*Institute of Quantum Optics, Leibniz University Hannover, Welfengarten 1, 30167 Hannover, Germany*

<sup>2</sup>*Max Born Institute, Max-Born-Str. 2a, 12489 Berlin*

<sup>3</sup>*Cluster of Excellence PhoenixD (Photonics, Optics, and Engineering - Innovation Across Disciplines), Welfengarten 1, 30167 Hannover, Germany*

<sup>4</sup>*Institute of Photonics, Leibniz University Hannover, Nienburgerstr. 17, 30519 Hannover*

(Dated: February 8, 2024)

Photons, acting as “flying qubits” in propagation geometries such as waveguides, appear unavoidably in the form of wavepackets (pulses). The actual shape of the photonic wavepacket, as well as possible temporal/spectral correlations between the photons, play a critical role in successful scalable computation. Currently, unentangled indistinguishable photons are considered as a suitable resource for scalable photonic circuits. Here we show that using so called coherent photon conversion, it is possible to construct flying-qubit gates, which are not only insensitive to waveshapes of the photons and temporal/spectral correlations between them, but which also fully preserve these waveshapes and correlations upon the processing. This allows using photons with correlations and purity in a very broad range for a scalable computation. Moreover, such gates can process entangled photonic wavepackets even more effectively than unentangled ones.

Despite photons being seemingly ideal candidates for carrying quantum information, robust scalable gates and circuits for the photonic qubits remain yet illusive. The difficulty is that photons do not interact to each other directly, and thus either indirect interaction via a nonlinear medium [1–12] or “emulation” of interaction using measurements [13–16] are needed. The waveshapes either in time [17–21] or in frequency [22–24] (or both together [25]) may themselves represent qubits. Alternatively, information can be stored in degrees of freedom orthogonal to waveshapes, such as which-path [15], polarization [15], field quadratures [26, 27] or angular momentum [28]. In all cases, regardless of the used approach, the shape of the photonic wavepacket is of primary importance for the gate action.

One ideally would desire a gate, working with (almost) arbitrary photonic waveshapes and fully preserve them during the computation – even if the waveshapes are not unentangled or not pure. We will call such gates “waveshape tolerant”. Formally speaking, waveshape tolerantness is a quite strong property; For instance, if we delay one of the two photons in a two-photon gate so that they do not overlap in time anymore, the waveshape tolerant gate should still work. Are such gates possible at all?

In linear optical circuits (LOC) [13–16] which consist of linear interferometric networks and measurements of ancillary qubits, it is known [29, 30] that for scalable operation the photons in different channels have to be independent and indistinguishable, so that no which-path information can be extracted, since its presence breaks the interference in linear optical elements, and introduces incoherence during measurements [29–31]. Although the action of LOC was recently extended to more general class of states [31], they certainly are not waveshape tolerant in the sense mentioned above.

The situation seems even worse if we consider a re-

cent proposal based on so called coherent photon conversion (CPC), where the photon-photon interaction is based on a four wave mixing (FWM) process in presence of a strong coherent laser field [1]. This coherent field amplifies the action of the  $\chi^{(3)}$  nonlinearity between the remaining three waves which are in a Fock state. A two-photon wavepacket sent to the input of a CPC device should experience up-/down-conversion cycles, attaining additional phase shift of  $\pi$  after each cycle, thus leading to a nonlinear sign (NS) gate functionality. Unfortunately, soon after the discovery of this approach it was noted [4] that if a finite size of the wavepackets is taken into account, it does not work even if the participating photons are temporally unentangled and indistinguishable, since only the parts of the bi-photon wavepacket located at the same position in space (or time) can effectively interact. This problem can be however solved if the photons have nonzero group velocity relative to each other [2, 5]. In this case, parts of the photons which were initially separated, eventually cross, and can interact at that moment. This approach was very recently partially realized experimentally [8] in a system with electromagnetic-induced transparency, however at the cost of partial loss of “working” photons. Besides, three photon interaction was observed in cold Rydberg atoms [32].

Nevertheless, with or without a relative movement of the photonic wavepackets, it seems at the first sight, that the CPC-based approach has no chances to produce waveshape tolerant gates, since, by up-conversion of a bi-photon wavepacket (described by a two-dimensional distribution) into a single photon (described by a one-dimensional waveform), some information about the initial two-photon waveshape is unavoidably lost, and the back-conversion cannot restore it anymore. Therefore, the final waveshape seemingly can coincide with the ini-

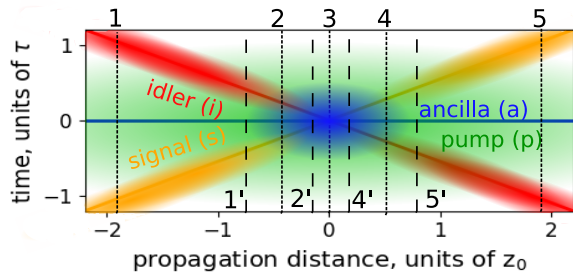


FIG. 1. CPC-based nonlinear sign (NS) gate with group-velocity-unmatched pulses. Single photon wavepackets denoted as ancilla ( $a$ , blue), signal ( $s$ , orange) and idler ( $i$ , red) propagate in presence of strong coherent pump ( $p$ , green), interacting via the FWM process. The moving centers of the wavepackets are indicated by solid lines. Color change denotes schematically conversion of photons. Vertical lines and numbers correspond to the positions of the snapshots shown in Fig. 2 (lines labeled 1-5 refer to S1,S2,S4, lines labeled 1',2',3,4',5' refer to S3).

tial one only by chance.

Despite of these objections, here we show that CPC-based gates can indeed possess the property of being wave-shape tolerant, if the wavepacket is slowly varying on the time scale of the effective photon-photon interaction, or, equivalently, if the suitable fourth-order coherence time is large enough. This implies also scalability of the gates to many entangled photons, as well as their ability to work with mixed states. Moreover, we show that processing of time- and frequency-entangled photons can be more efficient than of the unentangled ones.

*The model.* The CPC approach with group velocity-unmatched pulses proposed in [2] is shown in Fig. 1. The photons in Fock states at frequencies  $\omega_s$ ,  $\omega_i$ ,  $\omega_a$ , which we call signal ( $s$ ), idler ( $i$ ), and ancilla ( $a$ ), respectively, the first two (inspired by  $\chi^{(2)}$  terminology [33]), interact via the FWM process described by the susceptibility  $\chi^{(3)} = \chi^{(3)}(\omega_a; \omega_p, \omega_s, \omega_i)$  in presence of a strong coherent field ( $p$ ) at frequency  $\omega_p$  with the peak electric field  $E_p$ . This induces an effective three wave mixing (TWM) interaction between the  $a$ ,  $s$  and  $i$  wavepackets. Each of the wavepackets is described by the frequency-dependent operators  $a_a(\omega_a)$ ,  $a_s(\omega_s)$  and  $a_i(\omega_i)$ .

Since only parts of the wavepackets which are close to each other (in space or time) can interact, one has to resolve the finite size of the interaction region [2]. In the previous considerations [2, 5], the Hamiltonian containing spatial nonlocality was used for this purpose, attracting however critics as physically nontransparent [5]. Here we operate instead in terms of non-instantaneous response, that is, with nonlocality in time rather than in space, which is more physically justified (see [34] and also below), leading nevertheless to a formulation rather equivalent to [2, 5] in our particular case. The non-instantaneous interaction can be represented with a

Hamiltonian

$$H = \hbar\gamma' \int \tilde{h}(\omega_a, \omega_s, \omega_i) a_s^\dagger(\omega_s) a_i^\dagger(\omega_i) a_a(\omega_a) \times \\ \times d\omega_s d\omega_i d\omega_a + \text{h.c.} \quad (1)$$

Here  $\hbar$  is the Planck constant,  $\gamma' \sim \chi^{(3)} E_p$  is the interaction strength (see more details below, after Eqs. (5)-(4)), and  $\tilde{h}$  describes the non-instantaneous response of the nonlinear medium in frequency domain. Although our further analysis shows that the particular form of  $\tilde{h}$  is not important, for numerical simulations we use the function

$$\tilde{h}(\omega_a, \omega_s, \omega_i) = \frac{\delta(\omega_p - \omega_a + \omega_s + \omega_i)}{2\pi} e^{-\sigma^2(\omega_s^2 + \omega_i^2)/2}, \quad (2)$$

where  $\delta$  is the Dirac  $\delta$ -function. This response function has a transparent physical meaning:  $\delta$ -function ensures the energy conservation; The frequency-dependent form-factor effectively “switches off” the interaction at frequencies larger than  $\omega_R \approx 2\pi/\sigma$ . This represents schematically a typical frequency-dependent  $\chi^{(3)}$  for dielectrics [33–35], which vanishes at frequencies above the band-gap. The presence of the cutoff frequency  $\omega_R$  in Eq. (2) means that the photons can effectively interact to each other only if they are separated in time by an interval smaller than  $\sigma$ . This implies also spatial nonlocality: The photons interact if they are at the distance smaller than  $c\sigma$ . For “typical” materials like fused silica  $\sigma$  has been recently measured to be at the level of hundreds of attoseconds [36, 37].

The equation of motion can be written in the form of the Schrödinger equation  $i\hbar\partial_t |\Psi\rangle = (H_0 + H) |\Psi\rangle$ , where  $H_0$  is the non-interacting Hamiltonian. It is useful to formulate the corresponding wavevector  $|\Psi\rangle$  in terms of temporal modes [19]:

$$|\Psi\rangle = \int \int \Psi_{si}(t_s, t_i, z) |t_s\rangle_s |t_i\rangle_i dt_s dt_i + \\ + \int \Psi_a(t_a, z) |t_a\rangle_a dt_a, \quad (3)$$

where  $|t_j\rangle_j = \int e^{it_j\omega_j} a_j^\dagger(\omega_j) |0\rangle_{\omega_j} d\omega_j$ ,  $j = \{s, i\}$ ,  $|t_a\rangle_a = \int e^{it_a(\omega_a - \omega_p)} a_a^\dagger(\omega_a) |0\rangle_{\omega_a} d\omega_a$ , where  $a^\dagger$  and  $|0\rangle$  denote creation operators and vacuum states for the corresponding modes and frequencies. Also, we assume that the higher order linear dispersion is negligible leading to  $H_0 = \sum_j \hbar \int \omega a_j^\dagger(\omega) a_j(\omega) d\omega + \text{h.c.}$  (see Supplementary).

This allows us to write down the evolution equations for  $\Psi_{si}(t_s, t_i, z)$ ,  $\Psi_a(t_a, z)$  in  $z$ -direction in space, assuming 1D propagation geometry such as for example in waveguides.  $t$ - and  $z$ -formulations are mathematically equivalent in our case [38] (no higher order dispersion and small group mismatch, see Supplementary for more details). The resulting equations written in the frame of reference propagating with the group velocity of the ancilla  $v_a$  are:

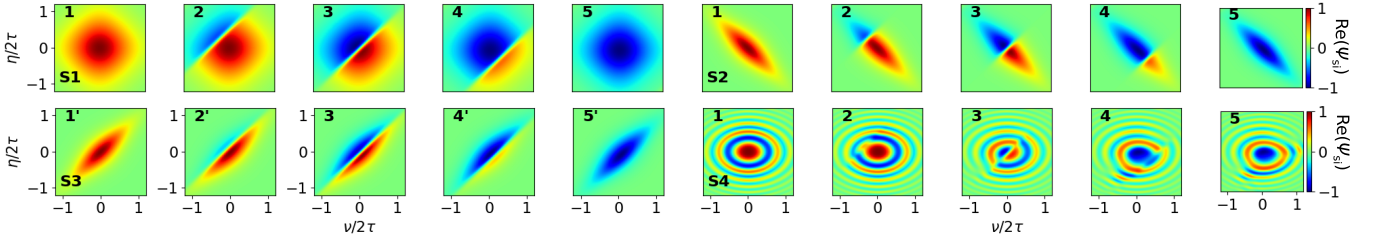


FIG. 2. Snapshots of the signal idler wavepacket represented by  $\text{Re}(\Psi_{\text{si}}(t_s, t_i, z))$  for different initial wavelshapes marked as S1...S4 (see text) shown in the moving coordinates  $\eta = (t_s - z\beta_{1s})$ ,  $\nu = (t_i - z\beta_{1i})$ . The positions of the snapshots in  $z$  are indicated in Fig. 1 by the vertical lines and corresponding numbers. Sign flip of  $\text{Re}(\Psi_{\text{si}})$  indicates successful NS gate operation. The wavelshapes in S1...S3 are fully conserved, which is not the case for S4 where distortions appear.

$$\frac{\partial \Psi_{\text{si}}(t_s, t_i, z)}{\partial z} = -\beta_{1s} \frac{\partial \Psi_{\text{si}}(t_s, t_i, z)}{\partial t_s} - \beta_{1i} \frac{\partial \Psi_{\text{si}}(t_s, t_i, z)}{\partial t_i} - i\gamma \int h(t_a, t_s, t_i) \Psi_a(t_a, z) dt_a, \quad (4)$$

$$\frac{\partial \Psi_a(t_a, z)}{\partial z} = -i\gamma \iint h(t_a, t_s, t_i) \Psi_{\text{si}}(t_s, t_i, z) dt_s dt_i. \quad (5)$$

Here  $\beta_{1j} = 1/v_j - 1/v_a$ ,  $j = \{s, i\}$ ,  $v_j$  are the corresponding group velocities,  $h(t_a, t_s, t_i)$  is the Fourier transform of  $\tilde{h}(\omega_a, \omega_s, \omega_i)$ :

$$h(t_a, t_s, t_i) = \frac{1}{2\pi\sigma^2} e^{-(t_s - t_a)^2/2\sigma^2} e^{-(t_i - t_a)^2/2\sigma^2}. \quad (6)$$

$\gamma \approx \gamma'/\sqrt{v_a}$  can be obtained from the limit of instantaneous nonlinearity [39] (see details in Supplementary) as  $\gamma = \hbar\omega_p^2 n_2 \Phi_p / cS$ , where  $S$  is the effective area of the beam (assumed to be the same for all waves),  $c$  is the speed of light in vacuum,  $\Phi_p = \sqrt{I_p / \hbar\omega_p}$ ,  $I_p$  is the intensity of  $p$ , and  $n_2$  corresponds to  $\chi^{(3)}$  of the relevant FWM process.

*Numerical simulations.* In numerical simulations we assumed  $\beta_{1s} = -\beta_{1i} \equiv \beta_1$ , that is, the signal and idler pulses propagate with equal velocities of opposite sign in the frame of reference of the ancilla (see Fig. 1). If we denote the initial pulse duration by  $\tau$ , the effective overlap (and thus interaction) of the signal and idler wavelshapes takes place over the distance  $\approx z_0$ , where  $z_0 = \tau/\beta_1$ . For the sake of generality, we normalized time  $t$  to  $\tau$  and  $z$  to  $z_0$ , leading to the following renormalizations in Eqs. (4)-(5):  $\beta_{1j} \rightarrow 1$  for  $j = \{s, i\}$ ,  $\hbar\gamma \rightarrow \hbar\gamma/\beta_1$ ,  $\Psi_a \rightarrow \Psi_a/\sqrt{z_0}$ ,  $\Psi_{\text{si}} \rightarrow \Psi_{\text{si}}/z_0$ . Numerical simulations were made in the range  $z = [-L/2, L/2]$  for  $L = 4.4z_0$  (see Fig. 1). We initialized our wavelshapes at  $z = -L/2$  with the vacuum for the ancilla ( $\Psi_a = 0$ ) and two photons in signal and idler modes with various initial distributions  $\Psi_{\text{si}}(t_s, t_i, -L/2) = \Psi^{(\text{in})}(t_s, t_i)$  for four different simulations denoted as S1...S4 in Fig. 2. For the simulations S1, S2, S3 we used the wavelshape

$$\Psi^{(\text{in})}(t_s, t_i) = \Psi_0 \mathcal{R}_\phi \left[ \text{sech} \left( \frac{t_s - t_{s0}}{\tau_s} \right) \text{sech} \left( \frac{t_i - t_{i0}}{\tau_i} \right) \right],$$

where  $\Psi_0$  is a normalization factor leading to  $\|\Psi_{\text{si}}(t_s, t_i, -L/2)\| = 1$  (here  $\|f\|$  is the norm of a function  $f$ :  $\|f\| = \int \int f(x, y) dx dy$ ),  $\mathcal{R}_\phi$  is the transformation rotating  $\Psi(t_s, t_i)$  in  $(t_s, t_i)$  plane by the angle  $\phi$ . For S1 we used (in normalized units mentioned above)  $\tau_s = \tau_i = 1$ ,  $\phi = 0$  which gives the separable wavelshape, and  $t_{s0} = -1.2\tau_s$ ,  $t_{i0} = 1.2\tau_s$ . For S2 and S3 we assumed  $\tau_s = 1$ ,  $\tau_i = 1/3$  (in normalized units);  $\phi = \pi/4$  for S2 and  $\phi = -\pi/4$  for S3, constructing thereby two states with signal and idler being entangled. Finally, in S4 we assumed the initial distribution as in S1 but modified by multiplying  $\Psi(t_s, t_i, -L/2)$  by the time dependent factor  $\exp(iC_s t_s^2 + iC_i t_i^2)$  with  $C_s = C_i/2 = 10$ , introducing a time-dependent chirp into both signal and idler pulses. In simulations, we used  $\sigma/\tau = 0.05$ . As a ‘‘reference case’’ we take a fused silica waveguide with  $n_2 = 3 \times 10^{-16}$  cm<sup>2</sup>/W,  $S = 1 \mu\text{m}^2$ . We also assume  $\sigma$  of 500 attoseconds (as), which is of the order of values measured recently [36, 37]. The normalized parameters mentioned above correspond then to  $I_p = 20$  TW/cm<sup>2</sup> and FWHM duration of 10 fs ( $\tau = 5.4$  fs). The interaction distance is then on the kilometer range: taking  $z_0 = 3$  km ( $\beta_1 = 1.8$  fs/km) leads to the fidelity  $\mathcal{F} = 99\%$ . On the other hand, faster than optimal propagation reduces back-conversion and thus fidelity; for instance, increasing  $\beta_1$  two times leads to  $\mathcal{F} = 90\%$ . We note furthermore that the gate length is inversely proportional to  $n_2/S$ ; Using of novel photonic materials [40–45], such as silicon, noncrystalline diamond and others may reduce the gate length to a centimeter range. For further discussion of these issues see Supplementary.

The results of simulations are shown in Fig. 2 as snapshots of  $\text{Re} \Psi_{\text{si}}(t_s, t_i, z)$  at the positions marked by 1...5

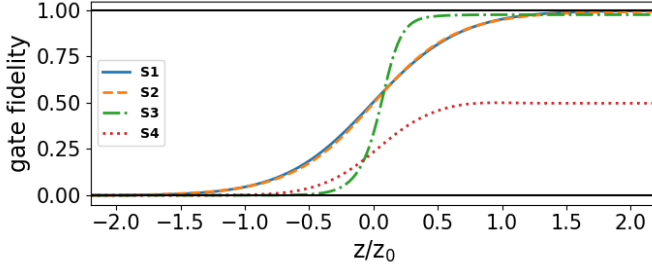


FIG. 3. Evolution of the gate fidelity  $\mathcal{F}(z)$  for the simulations S1...S4 in Fig. 2.

(for S1...S3) and 1', 2', 3, 4', 5' (for S3) in Fig. 1 by vertical lines. A successful gate operation assumes the phase change of  $\pi$ , which means sign flip of  $\text{Re } \Psi_{\text{si}}(t_s, t_i, z)$ . As one can see in Fig. 2, the gate operation takes place in a form of a “front” of the size  $\sim \sigma$  which moves through the wavelshape. In the case S3 the interaction is completed at around 3 times shorter distance corresponding to the 3 times smaller duration of the wavepacket in the direction of the front movement. Interestingly, at the point “3” we have a Bell-type state  $|+\rangle_s |+\rangle_i - |-\rangle_s |-\rangle_i$ , where  $|\pm\rangle_j$  denotes the signal ( $j = s$ ) or idler ( $j = i$ ) photon, located in upper-left (+) or lower-right (-) corner of the  $(\nu, \eta)$  plain.

The quality of the gate operation and its ability to keep the wavelshape can be quantified by the fidelity  $\mathcal{F}$  presented in Fig. 3 and defined as  $\mathcal{F}(z) = \frac{1}{2} \left| 1 - \int \int \Psi_{\text{si}}^{(\text{norm})}(t_s, t_i, z) \Psi_{\text{si}}^{(\text{in})*}(t_s, t_i) dt_s dt_i \right|$ , where  $\Psi_{\text{si}}^{(\text{norm})}(t_s, t_i, z) = \Psi_{\text{si}}(t_s, t_i, z) / \|\Psi_{\text{si}}(t_s, t_i, z)\|$ .  $\mathcal{F} = 1$  corresponds to a perfect gate operation, including full conservation of the pulse shape. One can see indeed from Fig. 2 and Fig. 3, that for the cases S1, S2, S3 not only the phase is successfully flipped, but the wavelshape also remains intact after the gate. On the other hand, the phase deformation introduced in (S4) makes the wavelshape changing quickly on the scale of  $\sigma$ , leading to a visibly corrupted wavelshape reflected in the low fidelity in Fig. 3.

Summarizing, smooth enough wavepackets are processed in a wavelshape tolerant way. On the other side, processing of wavelshapes with features, “sharp” on the scale of  $\sigma$ , is not anymore perfect.

*Analytics.* We proceed further with a more general analytical insight. We derive the equation describing evolution of the wavepacket  $\Psi_{\text{si}}$  for an arbitrary response function  $h$  localized mostly in the region of the size  $\approx \sigma \times \sigma$  of the point  $t_s = t_i$  and being symmetric in respect to its maxima ( $h$  used above is a particular example of such function), whereas  $\Psi_{\text{si}}$  is slow on the scale of  $\sigma$ , meaning:

$$|\partial_{t_j} \Psi_{\text{si}}(t_s, t_i, z)| \ll |\Psi_{\text{si}}(t_s, t_i, z)| / \sigma \quad (7)$$

for  $j = \{s, i\}$  for all  $t_s, t_i$ . Under these conditions, the

equation describing the evolution of a small part  $\delta\Psi$  of the size  $\sigma \times \sigma$  of the whole wavepacket  $\Psi_{\text{si}}$  is described by (see Supplementary for more details):

$$\partial_{\xi\xi} \delta\Psi(\xi, \eta, \nu) + \frac{\gamma^2}{\sigma} K(\xi - \xi_0) \delta\Psi(\xi, \eta, \nu) = 0, \quad (8)$$

where  $\xi = \beta_1(z - t_i/\beta_{1i} + t_s/\beta_{1s})$ ,  $\eta = (t_s - z\beta_{1s})$ ,  $\nu = (t_i - z\beta_{1i})$ ,  $K(\xi - \xi_0)$  is a coupling factor which is of the order of one close to  $\xi = \xi_0$  and quickly approaches zero as  $|\xi - \xi_0|$  becomes larger than  $\sigma$  (that is, we leave the  $\sigma$  vicinity of  $\xi_0$ ). For instance, for a  $h$  given by Eq. (6) we have  $K(\xi - \xi_0) \propto \exp(-(\xi - \xi_0)^2/4\sigma^2)$ .

Eq. (8) is an equation for a harmonic oscillator with variable frequency. In the interaction region of the size  $\sigma$  near  $\xi = \xi_0$  the harmonic oscillator (and thus the conversion) is effectively switched on, and outside, it is off. This region defines the conversion front visible in Fig. 2. For the perfect gate operation, exactly half of an oscillation period is necessary. Since Eq. (8) is linear, and the evolution starts from the same initial phase ( $\Psi_{\text{si}}$  is at maximum) in all points  $(\eta, \nu)$ , the same part of oscillation is performed everywhere, making the shape of  $\Psi_{\text{si}}$  preserved.

Importantly, this result is general in the sense that it applies for any  $\Psi_{\text{si}}$  satisfying the slowness condition Eq. (7), also for arbitrary noninstantaneous response  $h$  satisfying the conditions mentioned above. S4 in Fig. 2 shows that if this condition is not satisfied, the gate may indeed modify the wavepacket shape, since the noninstantaneous interaction mix different pieces of the wavelshape.

*Scalability and operation for mixed states.* Here we show, that the NS gate works properly for mixed states (described by a density matrix  $\rho_{\text{si}}$ ), if a more general slowness condition is satisfied. We sketch the consideration, technical details can be found in the Supplementary.  $\rho_{\text{si}}$  can always be represented as a pure state  $|\Psi\rangle$  in some “larger” space [46]. In our case,  $|\Psi\rangle$  can be represented as a sum of orthogonal contributions with amplitudes given by a set of “partial wavelshapes”  $\Psi_{\text{si}}^{\{w\}}(t_s, t_i)$ , describing the signal-idler state in each of the configurations  $\{w\}$  of the rest of that larger space. Every of  $\Psi_{\text{si}}^{\{w\}}$  evolves fully independently from the others, and obey the same Schrödinger equation Eqs. (4)-(5). Therefore,  $\rho_{\text{si}}$  will be processed correctly if all of  $\Psi_{\text{si}}^{\{w\}}$  satisfy the slowness condition Eq. (7).

Furthermore, using the fourth-order coherence function  $\Gamma^{(2,2)}$  [47]

$$\Gamma^{(2,2)}(\tau_s, \tau_i) = \text{tr} \left( \rho_{\text{si}} a_s^\dagger(t_s - \tau_s) a_i^\dagger(t_i - \tau_i) a_s(t_s) a_i(t_i) \right),$$

Eq. (7) can be reformulated in an equivalent form:

$$\Gamma^{(2,2)}(\tau_s, \tau_i) \approx \Gamma^{(2,2)}(0, 0) \quad (9)$$

for  $|\tau_s| \lesssim \sigma$ ,  $|\tau_i| \lesssim \sigma$ . Eq. (9) obviously can not be satisfied if  $\mathcal{T}^{(4)} \lesssim \sigma$ , where  $\mathcal{T}^{(4)}$  is the coherence time defined

by the width of  $\Gamma^{(2,2)}(\tau_s, \tau_i)$ , so the opposite condition,

$$\mathcal{T}^{(4)} \gg \sigma, \quad (10)$$

is therefore necessary for the validity of Eq. (9). Except some pathological waveshapes,  $\Gamma^{(2,2)}$  decreases monotonously near the origin  $(\tau_s, \tau_i) = (0, 0)$ . Thus, in most cases,  $\mathcal{T}^{(4)} \gg \sigma$  delivers also the sufficient condition and can be therefore considered as a suitable criterion for the proper gate operation.

*Discussion and conclusions.* We showed that CPC-based gates can be "waveshape tolerant", that is, successfully process arbitrary waveshapes keeping them intact, if the waveshapes vary slowly on the timescale of  $\sigma$ , the noninstantaneous response time of the nonlinearity. This condition can be reformulated in the form of a constraint on the fourth order coherence given by Eq. (9), or, in the most cases, as an even simpler condition Eq. (10) on the corresponding coherence time, both applicable also to mixed states. Importantly, since the pulses cross each other, also temporal offsets are processed correctly if the available propagation length is large enough (see Supplementary for more details on this).

The smallest  $\sigma$  appear for off-resonant nonlinearities such as in fused silica at optical frequencies, in which case it lies in the attosecond range [36, 37]. Our simulations indicate that in this situation the gate operation is not impossible, if a strong coherent pump in the TW/cm<sup>2</sup> range and pulse durations in the femtosecond range are used, assuming that the waveguide dispersion is managed properly and the frequency channels are well separated.

We remark that the slowness condition mentioned above is a very strong property. Most waveshapes changing slowly on the scale of the working wavelength  $\lambda$  and thus on the scale of  $\sigma$ , since most typically  $\sigma \lesssim \lambda$  in optics. It is thus notoriously difficult to produce experimentally a waveshape which breaks this condition. In more complex logical circuits, limitation due to linear optical elements become even more strict, since even ideal linear optical elements are known to preserve only symmetric distributions (like  $\Psi_{\text{si}}(t_s, t_i) = \Psi_{\text{si}}(t_i, t_s)$ ) [29].

Waveshape tolerantness relaxes significantly the requirements to the photon sources needed for scalable computing. The photons do not need to be indistinguishable, unentangled or even pure anymore. Moreover, as we have seen, some entangled distributions promise an significant advantage in the resulting gate size over the uncorrelated photons.

I.B. and U.M. thank Deutsche Forschungsgemeinschaft (DFG, German Research Foundation), projects BA 4156/4-2 and MO 850-19/2 for support. I.B., A.D., M.K., and U.M. acknowledge support from Germany's Excellence Strategy within the Cluster of Excellence EXC 2122 PhoenixD (Project ID 390833453) and Germany's Excellence Strategy EXC-2123 QuantumFrontiers (Project ID 390837967). M.K acknowledges sup-

port from the German ministry of education and research (PQuMAL project).

- 
- [1] N. K. Langford, S. Ramelow, R. Prevedel, W. J. Munro, G. J. Milburn, and A. Zeilinger, Efficient quantum computing using coherent photon conversion, *Nature* **478**, 360 (2011).
  - [2] K. Xia, M. Johnsson, P. L. Knight, J. Twamley, Cavity-free scheme for nondestructive detection of a single optical photon, *Phys. Rev. Lett.* **116**, 023601 (2016).
  - [3] M. Y. Niu, I. L. Chuang, and J. H. Shapiro, Qudit-basis universal quantum computation using  $\chi^{(2)}$  interactions, *Phys. Rev. Lett.* **120**, 160502 (2018).
  - [4] B. Viswanathan and J. Gea-Banacloche, Multimode analysis of a conditional phase gate based on second-order nonlinearity, *Phys. Rev. A* **92**, 042330 (2015).
  - [5] B. Viswanathan and J. Gea-Banacloche, Analytical results for a conditional phase shift between single-photon pulses in a nonlocal nonlinear medium, *Phys. Rev. A* **97**, 032314 (2018).
  - [6] M. Kounalakis, C. Dickel, A. Bruno, N. K. Langford, and G. A. Steele, Tuneable hopping and nonlinear cross-kerr interactions in a high-coherence superconducting circuit, *npj Quantum Inf.* **4**, 1 (2018).
  - [7] D. Tiarks, S. Schmidt-Eberle, T. Stolz, G. Rempe, and S. Dürr, A photon-photon quantum gate based on rydberg interactions, *Nature Physics* **15**, 124 (2019).
  - [8] S. Sagona-Stophel, R. Shahrokhshahi, B. Jordaán, M. Namazi, and E. Figueroa, Conditional  $\pi$ -phase shift of single-photon-level pulses at room temperature, *Phys. Rev. Lett.* **125**, 243601 (2020).
  - [9] M. Heuck, K. Jacobs, and D. R. Englund, Controlled-phase gate using dynamically coupled cavities and optical nonlinearities, *Phys. Rev. Lett.* **124**, 160501 (2020).
  - [10] Audrey Dot, Evan Meyer-Scott, Raja Ahmad, Martin Rochette, and Thomas Jennewein, "Converting one photon into two via four-wave mixing in optical fibers," *Phys. Rev. A* **90**, 043808 (2014).
  - [11] Evan Meyer-Scott, Audrey Dot, Raja Ahmad, Lizhu Li, Martin Rochette, and Thomas Jennewein, "Power-efficient production of photon pairs in a tapered chalcogenide microwire," *Applied Physics Letters* **106**, 081111 (2015).
  - [12] Alexander S. Solntsev, Sergey V. Batalov, Nathan K. Langford, and Andrey A. Sukhorukov, "Complete conversion between one and two photons in nonlinear waveguides with tailored dispersion," (2021), arXiv:2110.03110 [physics.optics].
  - [13] E. Knill, R. Laflamme, and G. J. Milburn, A scheme for efficient quantum computation with linear optics, *Nature* **409**, 46 (2001).
  - [14] J. L. O'Brien, G. J. Pryde, A. G. White, T. C. Ralph, and D. Branning, Demonstration of an all-optical quantum controlled-not gate, *Nature* **426**, 264 (2003).
  - [15] P. Kok, W. J. Munro, K. Nemoto, T. C. Ralph, J. P. Dowling, and G. J. Milburn, Linear optical quantum computing with photonic qubits, *Rev. Mod. Phys.* **79**, 135 (2007).
  - [16] J. Carolan, C. Harrold, C. Sparrow, E. Martín-López, N. J. Russell, J. W. Silverstone, P. J. Shadbolt, N. Mat-

- suda, M. Oguma, M. Itoh, G. D. Marshall, M. G. Thompson, J. C. F. Matthews, T. Hashimoto, J. L. O'Brien, and A. Laing, Universal linear optics, *Science* **349**, 711 (2015).
- [17] I. Marcikic, H. de Riedmatten, W. Tittel, V. Scarani, H. Zbinden, and N. Gisin, Time-bin entangled qubits for quantum communication created by femtosecond pulses, *Phys. Rev. A* **66**, 062308 (2002).
- [18] C. Xiong, X. Zhang, A. Mahendra, J. He, D.-Y. Choi, C. J. Chae, D. Marpaung, A. Leinse, R. G. Heideman, M. Hoekman, C. G. H. Roeloffzen, R. M. Oldenbeuving, P. W. L. van Dijk, C. Taddei, P. H. W. Leong, and B. J. Eggleton, Compact and reconfigurable silicon nitride time-bin entanglement circuit, *Optica* **2**, 724 (2015).
- [19] B. Brecht, D. V. Reddy, C. Silberhorn, and M. G. Raymer, Photon temporal modes: a complete framework for quantum information science, *Phys. Rev. X* **5**, 041017 (2015).
- [20] V. Ansari, J. M. Donohue, B. Brecht, and C. Silberhorn, Tailoring nonlinear processes for quantum optics with pulsed temporal-mode encodings, *Optica* **5**, 534 (2018).
- [21] K.-H. Luo, S. Brauner, C. Eigner, P. R. Sharapova, R. Ricken, T. Meier, H. Herrmann, and C. Silberhorn, Nonlinear integrated quantum electro-optic circuits, *Science Advances* **5**, 10.1126/sciadv.aat1451 (2019).
- [22] S. Ramelow, L. Ratschbacher, A. Fedrizzi, N. K. Langford, and A. Zeilinger, Discrete tunable color entanglement, *Phys. Rev. Lett.* **103**, 253601 (2009).
- [23] L. Olislager, J. Cussey, A. T. Nguyen, P. Emplit, S. Massar, J.-M. Merolla, and K. P. Huy, Frequency-bin entangled photons, *Phys. Rev. A* **82**, 013804 (2010).
- [24] C. Reimer, M. Kues, P. Roztocki, B. Wetzal, F. Grazioso, B. E. Little, S. T. Chu, T. Johnston, Y. Bromberg, L. Caspani, D. J. Moss, and R. Morandotti, Generation of multiphoton entangled quantum states by means of integrated frequency combs, *Science* **351**, 1176 (2016).
- [25] M. Kues, C. Reimer, P. Roztocki, L. R. Cortés, S. Sciara, B. Wetzal, Y. Zhang, A. Cino, S. T. Chu, B. E. Little, *et al.*, On-chip generation of high-dimensional entangled quantum states and their coherent control, *Nature* **546**, 622 (2017).
- [26] S. L. Braunstein and P. van Loock, Quantum information with continuous variables, *Rev. Mod. Phys.* **77**, 513 (2005), quant-ph/0410100.
- [27] U. Andersen, G. Leuchs, and C. Silberhorn, Continuous-variable quantum information processing, *Laser & Photon. Rev.* **4**, 337 (2010).
- [28] A. Mair, A. Vaziri, G. Weihs, and A. Zeilinger, Entanglement of the orbital angular momentum states of photons, *Nature* **412**, 313 (2001).
- [29] A. B. U'ren, K. Banaszek, and I. A. Walmsley, Photon engineering for quantum information processing, *Quantum Inf. Comput.* **3**, 480. 23 p (2003).
- [30] A. U'Ren, C. Silberhorn, K. Banaszek, I. Walmsley, R. Erdmann, W. Grice, and M. Raymer, Generation of pure-state single-photon wavepackets by conditional preparation based on spontaneous parametric downconversion, *Laser Phys.* **15** (2005).
- [31] I. Babushkin, U. Morgner, and A. Demircan, Stability of quantum linear logic circuits against perturbations, *J. Phys. A: Math. Theor.* **53**, 445307 (2020).
- [32] Q.-Y. Liang, A. V. Venkatramani, S. H. Cantu, T. L. Nicholson, M. J. Gullans, A. V. Gorshkov, J. D. Thompson, C. Chin, M. D. Lukin, and V. Vuletić, Observation of three-photon bound states in a quantum nonlinear medium, *Science* **359**, 783 (2018).
- [33] R. Boyd and M. Boyd, *Nonlinear Optics* (Academic Press, 1992).
- [34] N. Bloembergen, *Nonlinear Optics* (World Scientific, 1996).
- [35] C. Brée, *Nonlinear optics in the filamentation regime* (Springer Science & Business Media, 2012).
- [36] M. Hofmann, J. Hyyti, S. Birkholz, M. Bock, S. K. Das, R. Grunwald, M. Hoffmann, T. Nagy, A. Demircan, M. Jupé, D. Ristau, U. Morgner, C. Brée, M. Woerner, T. Elsaesser, and G. Steinmeyer, Noninstantaneous polarization dynamics in dielectric media, *Optica* **2**, 151 (2015).
- [37] A. Sommer, E. Bothschafter, S. Sato, C. Jakubeit, T. Latka, O. Razskazovskaya, H. Fattahi, M. Jobst, W. Schweinberger, V. Shirvanyan, *et al.*, Attosecond nonlinear polarization and light-matter energy transfer in solids, *Nature* **534**, 86 (2016).
- [38] N. Quesada, G. Triginer, M. D. Vidrighin, and J. E. Sipe, Theory of high-gain twin-beam generation in waveguides: From Maxwell's equations to efficient simulation, *Phys. Rev. A* **102**, 033519 (2020).
- [39] P. Drummond and M. Hillery, *The Quantum Theory of Nonlinear Optics* (Cambridge University Press, 2014).
- [40] G.P. Agrawal, *Nonlinear Fiber Optics*, 5th ed. (Elsevier, 2007).
- [41] J. Leuthold, C. Koos, and W. Freude, "Nonlinear silicon photonics," *Nature Photonics* **4**, 535–544 (2010).
- [42] Mari Motojima, Takara Suzuki, Hidemi Shigekawa, Yuta Kainuma, Toshi An, and Muneaki Hase, "Giant nonlinear optical effects induced by nitrogen-vacancy centers in diamond crystals," *Opt. Express* **27**, 32217–32227 (2019).
- [43] F. Trojánek, K. Židek, B. Dzurňák, M. Kozák, and P. Malý, "Nonlinear optical properties of nanocrystalline diamond," *Opt. Express* **18**, 1349–1357 (2010).
- [44] Tsuyoshi Michinobu, Joshua C May, Jin H Lim, Corinne Boudon, Jean-Paul Gisselbrecht, Paul Seiler, Maurice Gross, Ivan Biaggio, and François Diederich, "A new class of organic donor-acceptor molecules with large third-order optical nonlinearities," *Chemical communications*, 737–739 (2005).
- [45] Bweh Esembeson, Michelle L Scimeca, Tsuyoshi Michinobu, François Diederich, and Ivan Biaggio, "A high-optical quality supramolecular assembly for third-order integrated nonlinear optics," *Advanced materials* **20**, 4584–4587 (2008).
- [46] M. Nielsen and I. Chuang, *Quantum Computation and Quantum Information: 10th Anniversary Edition* (Cambridge University Press, 2010).
- [47] L. Mandel, E. Wolf, and C. U. Press, *Optical Coherence and Quantum Optics*, EBL-Schweitzer (Cambridge University Press, 1995).